JACS Au
AN OPEN ACCESS JOURNAL OF THE AMERICAN CHEMICAL SOCIETY

pubs.acs.org/jacsau

Article

Visible-Light-Driven Water Oxidation on Self-Assembled Metal-Free Organic@Carbon Junctions at Neutral pH

Astrid J. Olaya,* Julieta S. Riva, Dominika Baster, Wanderson O. Silva, François Pichard, and Hubert H. Girault*

Cite This: *JACS Au* 2021, 1, 2294–2302

Read Online

ACCESS | Metrics & More | Article Recommendations | Supporting Information

ABSTRACT: Sustainable water oxidation requires low-cost, stable, and efficient redox couples, photosensitizers, and catalysts. Here, we introduce the *in situ* self-assembly of metal-atom-free organic-based semiconductive structures on the surface of carbon supports. The resulting TTF/TTF$^{\bullet+}$@carbon junction (TTF = tetrathiafulvalene) acts as an all-in-one highly stable redox-shuttle/photosensitizer/molecular-catalyst triad for the visible-light-driven water oxidation reaction (WOR) at neutral pH, eliminating the need for metallic or organometallic catalysts and sacrificial electron acceptors. A water/butyronitrile emulsion was used to physically separate the photoproducts of the WOR, H^+ and TTF, allowing the extraction and subsequent reduction of protons in water, and the *in situ* electrochemical oxidation of TTF to TTF$^{\bullet+}$ on carbon in butyronitrile by constant anode potential electrolysis. During 100 h, no decomposition of TTF was observed and O_2 was generated from the emulsion while H_2 was constantly produced in the aqueous phase. This work opens new perspectives for a new generation of metal-atom-free, low-cost, redox-driven water-splitting strategies.

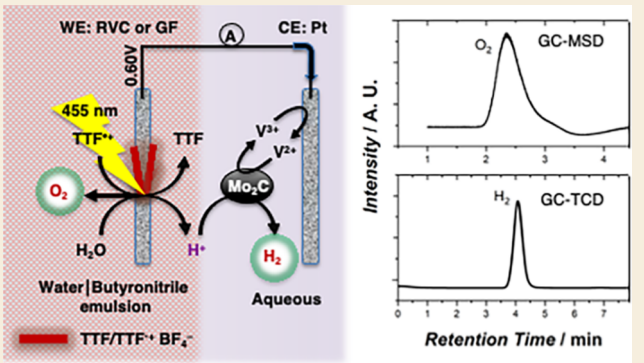

KEYWORDS: *water oxidation, hydrogen evolution, photochemistry, sustainable, redox shuttles*

INTRODUCTION

The increase of the global energy demand and the negative environmental impact triggered by the overexploitation of fossil fuels accentuate the need for the development of clean, efficient, and sustainable energy technologies.[1−18] Hydrogen is rapidly becoming the energy vector of choice, and advanced water electrolysis is one of the most efficient approaches to produce high-quality green H_2 from renewable energy sources despite their intermittencies.[1−3] To carry out what is often referred as artificial photosynthesis to produce hydrogen and oxygen directly from water, one usually combines an antenna such as a dye to absorb the light, a semiconductor to carry out the charge separation, and some electrocatalysts to drive both water reduction and the water oxidation reaction (WOR).[1−18] As of today, the photosensitized oxidation of water to oxygen under visible-light irradiation is still the bottleneck of artificial photosynthesis hindering large-scale developments. Light-driven water oxidation on semiconductor photoelectrodes has been extensively studied for nearly five decades with slow progress due to the difficulty of finding electrode materials exhibiting high chemical stability, suitable optoelectronic properties, and high catalytic efficiencies. Materials, such as titanium dioxide, absorbs only a very small part of the solar spectrum.[1−18] The sensitization of semiconductors has been significantly improved by using a wide range of metal complexes, organic dyes, and porphyrins.[4,12,14,17,19−26] Photocatalytic junctions based on $BiVO_4$, Fe_2O_3, WO_3, and Ag_3PO_4, among others, have been widely studied for water oxidation in both suspensions and photoelectrochemical devices.[8,10,27−33] Metal−molecule interactions play a key role in the water oxidation reaction.[34−36] However, the need for sacrificial electron acceptors such as Ag^+, Fe^{3+}, and peroxodisulfate ($S_2O_8^{2-}$) restricts its scalability.[37] Silicon and III−V compounds (GaAs, GaP, etc.) exhibit excellent optoelectronic properties but due to their instability under illumination in aqueous solutions, they require high-quality protective layers to prevent photocorrosion.[2]

On the molecular side, many organometallic compounds have been proposed as antennae and redox catalysts, but none have yet found industrial applications.[17] Nonetheless, it can also be noted that some fully organic compounds have been found to be electrocatalytically active for water oxidation on glassy-carbon or Pt working electrodes in the dark.[38−40]

Received: September 20, 2021
Published: November 11, 2021

https://doi.org/10.1021/jacsau.1c00408
JACS Au 2021, 1, 2294−2302

Due to their strong self-assembly properties, the radical cation of the organic electron donor tetrathiafulvalene ($TTF^{\bullet+}$) and its derivatives are frequently used as building blocks for the synthesis of highly electrically conducting structures.[34,41−43] Such properties have been extensively exploited to develop organic conductors, superconductors, photovoltaic cells, and solar cells, among others.[41−47] Metal−ligand coordination strategies have been widely used to create self-assembled three-dimensional TTF-based architectures where the $TTF^{\bullet+}$ sites enhance conductivity. Indeed, TTF-based metal−organic frameworks (MOFs) show an extended charge transport pathway within the rigid MOF structure,[48,49] exhibiting semiconductive properties comparable to that of common organic semiconductors.[48,49] Some examples include Zn_2(TTFTB) (10^{-6} S cm^{-1}), Co_2(TTFTB) (10^{-6} S cm^{-1}), Mn_2(TTFTB) (10^{-5} S cm^{-1}), and Cd_2(TTFTB) (10^{-4} S cm^{-1}), TB stands for tetrabenzoate.[48,49]

$(TTF)_3(BF_4)_2$ crystals are nonstoichiometric, with TTF moieties composed of TTF° monads interspersed with $(TTF^+)_2$ dyads stacked in parallel columns alternating with BF_4^- layers.[34,49,50] This salt behaves as an organic semiconductor, showing a conductivity of 2×10^{-5} S cm^{-1}.[34,49,50]

To overcome the efficiency, scale-up, and cost-related roadblocks of the conversion of solar energy into H_2 through photosensitized water splitting, the development of low-cost and highly stable photosensitizers/redox shuttles and photocatalysts is crucial. Furthermore, a system operating with water at neutral pH and without ion-exchange membranes is highly desirable.

Here, we introduce an efficient and highly stable visible-light-driven WOR by *in situ* self-assembled semiconductive tetrathiafulvalene-based structures ($TTF/TTF^{\bullet+}$) deposited on a solid carbon support. A water|butyronitrile emulsion was used as a platform for the spontaneous separation of the generated lipophilic TTF from the generated hydrophilic protons, with O_2 evolving as a gas. Such a separation allows the subsequent effective reduction of the protons to H_2 and the electrochemical recycling of the electron acceptor $TTF^{\bullet+}$.

EXPERIMENTAL SECTION

Synthesis of $TTF/TTF^{\bullet+}BF_4^-$

$TTF/TTF^{\bullet+}BF_4^-$ was synthesized entirely inside a glovebox purged with nitrogen by the stoichiometric oxidation of TTF (99%, Acros, structure in Scheme 1) with dry nitrosonium tetrafluoroborate ($NOBF_4$, 98%, Alfa Aesar) in dry butyronitrile (butyronitrile, 99.9%, Across). Prior to the reaction, butyronitrile was degassed in a Schlenk line and dried with molecular sieves (3 Å, Fisher Chemical) during 3 days inside of a glovebox. For the photochemical experiments, an excess of 5% of TTF was used in the synthesis of $TTF^{\bullet+}$ in order to consume any excess of oxidant, therefore avoiding oxidation of $TTF^{\bullet+}$ to TTF^{2+}. The resulting product in solution (Figure SI1) is further referred to as $TTF/TTF^{\bullet+}BF_4^-$. After the completion of the reaction, the solution was thoroughly degassed inside of a glovebox in order to evacuate the NO released during the reaction. The $TTF/TTF^{\bullet+}$ BF_4^- solution was always kept inside the glovebox and protected from the light.

Scheme 1. Chemical Structures of TTF, $HTTF^+$, and $TTF^{\bullet+}$

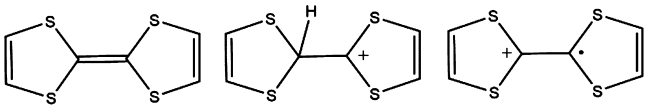

Cyclic Voltammetry (CV)

A three-electrode configuration composed of a commercial 3 mm diameter glassy-carbon electrode as the working electrode, Pt wire as the counter electrode, and an Ag/AgCl/3 M KCl double-junction reference electrode was used to analyze by CV 1 mM of the synthesized $TTF/TTF^{\bullet+}$ BF_4^- in 50 mM tetrabutylammonium tetrafluoroborate ($TBABF_4$, 99%, Acros) in butyronitrile. The scan rate was 10 mV s^{-1}. The CV (Figure SI1) was recorded inside a glovebox with a Metrohm Autolab PGSTAT 302N (Herisau, Switzerland) potentiostat.

For the electrochemical recycling of $TTF^{\bullet+}$ depicted in Scheme 2, CVs were recorded before and after the recycling to determine and verify the potential to be applied at the anode (WE). A glassy-carbon electrode (D = 3 mm) was used as the WE, and the scan rate was 25 mV $\cdot s^{-1}$.

Scheme 2. Visible-Light-Driven WOR by $TTF/TTF^{\bullet+}$@RVC or $TTF/TTF^{\bullet+}$@GF Junctions upon *In Situ* Electrochemical Recycling of $TTF^{\bullet+}$ and Continuous Reduction of Protons by V^{2+}/Mo_2C[a]

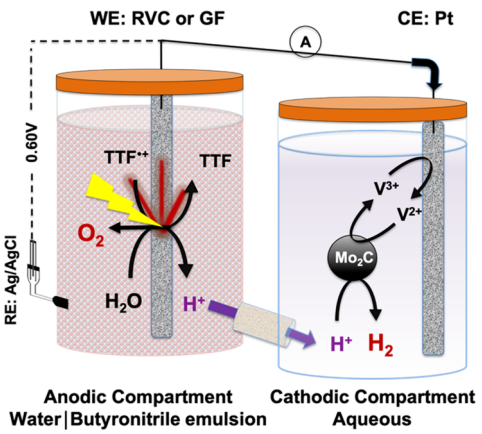

[a]Anodic compartment (left): organic phase (butyronitrile), 1 mM $TTF/TTF^{\bullet+}BF_4^-$ in 100 mM $TBABF_4$; aqueous phase, pure water. Anode, RVC or GF. Cathodic compartment (right): 100 mM VCl_2 in water, neutral pH, 40 mg of Mo_2C microparticles. Cathode: Pt mesh. The contents of the septum-sealed compartments were vigorously stirred, and the anodic compartment was illuminated with a 455 nm LED. Constant anode potential electrolysis of TTF: 0.6 V vs an Ag/AgCl/3 M KCl double-junction reference electrode. Bridge: glass wool plug to avoid butyronitrile from entering the cathodic compartment, while the two aqueous phases were kept in contact.

Visible-Light-Driven Water Oxidation by $TTF^{\bullet+}$*@Carbon Junctions during Constant Anode Potential Electrolysis of TTF Back to $TTF^{\bullet+}$ and Proton Extraction to Water for Reduction by V^{2+}/Mo_2C

The visible-light-driven WOR by $TTF/TTF^{\bullet+}$@carbon and the *in situ* electrochemical regeneration of $TTF^{\bullet+}$ were performed in the anodic compartment of the H-cell depicted in Scheme 2 (left side). The anode was illuminated with a 455 nm LED, and stirred inside of a glovebox filled with N_2. The protons resulting upon the WOR were spontaneously transferred to the aqueous phase and then to the cathodic compartment where they were reduced by V^{2+}/Mo_2C (Scheme 2, right side) by redox electrocatalysis.[36] The two septum-sealed compartments of the H-cell were separated by a glass wool plug, to avoid the mixing of $TTF^{\bullet+}$ and VCl_2. The glass wool plug ensured that the cathodic compartment was purely aqueous and that of the anodic compartment was a biphasic system kept as an emulsion during vigorous stirring.

The emulsion in the anodic compartment (left) was composed of 6 mL of 1 mM $TTF/TTF^{\bullet+}BF_4^-$ in 100 mM $TBABF_4$ in butyronitrile (organic phase) and 10 mL of pure water (aqueous phase). The pH of

https://doi.org/10.1021/jacsau.1c00408
JACS Au 2021, 1, 2294−2302

the emulsion was initially neutral. Two different carbon anodes (working electrode (WE)) were studied independently: reticulated vitreous carbon (RVC, Duocel) and graphite foil (GF, high-purity flexible graphite foil, SIGRAFLEX).

The cathodic compartment (right) contained 16 mL of 100 mM VCl_2 in water at neutral pH and 40 mg of Mo_2C microparticles (<10 μm). A Pt mesh (Sigma-Aldrich) was used as the cathode (counter electrode (CE)).

The reference electrode was an Ag/AgCl/3 M KCl double-junction electrode connected to the anodic compartment. The recycling potential of $TTF^{\bullet+}$ was set at 0.6 V vs the Ag/AgCl/3 M KCl double-junction reference electrode.

The gas products of the visible-light-driven WOR on the anodic side and the HER on the cathodic side were analyzed every 15 min by gas chromatography (GC-TCD-MS). Electrochemical impedance spectroscopy (EIS) under illumination was also performed every 15 min. To avoid overpressure of the system upon gas evolution, which in fact has a detrimental effect in the progress of the WOR and the HER, the recycling and illumination were paused after each GC and EIS analysis, and the cell was opened and degasified with N_2. Once the anode and the cathode did not show remanent O_2 or H_2, respectively, the cell was septum-sealed again and the WOR/electrochemical recycling/proton reduction was resumed.

Three control experiments were performed following the same methodology:

Control 1. without $TTF/TTF^{\bullet+}BF_4^-$ in the anodic compartment but with V^{2+}/Mo_2C in the cathodic compartment; GF as the anode and Pt mesh as the cathode.

Control 2. with $TTF/TTF^{\bullet+}$ BF_4^- in the anodic compartment but without V^{2+}/Mo_2C in the cathodic compartment; GF as the anode and Pt mesh as the cathode.

Control 3. carbon electrode replaced by platinum mesh with $TTF/TTF^{\bullet+}$ BF_4^- in the anodic compartment and with V^{2+}/Mo_2C in the cathodic compartment

For all three controls, the reference electrodes and all the other conditions were the same as for the system in Scheme 2. After every experiment the glass H-cell was washed with water, acid, and isopropanol. The carbon electrodes were new for each experiment.

Gas Chromatography (GC)

The headspaces of both septum-sealed compartments of the H-cell shown in Scheme 2 were sampled every 15 min by using a lock-in syringe with a push−pull valve (SGE Analytical Sciences). The gas was then injected into a TRACE 1300 GC equipped with a thermal conductivity detector (TCD) and an ISQ single quadrupole (mass spectrometry detector, MSD) from Thermo Fisher Scientific (GC-TCD-MSD). The chromatographic column was 5 Å molecular sieves, 80/100 mesh. Oxygen was detected with the MSD, using helium as the carrier gas, and H_2 was detected with the TCD, using argon as the carrier gas. The instrument was calibrated for O_2 and H_2 by using 8.0% and 0.8% O_2 in N_2 or H_2 in N_2 standards (99%, Carbagas). Prior to injection, the injection line was purged with N_2 and the exit of the line was connected to a water trap in order to avoid suction of air during the injections.

Electrochemical Impedance Spectroscopy (EIS)

Each EIS spectrum was recorded after every 15 min of electrolysis of TTF to $TTF^{\bullet+}$. Prior to impedance spectra recording, stirring was turned off such that the electrode was immersed only in the organic phase. Stirring was then resumed to continue the electrolysis. Conditions: 10 mV amplitude perturbation, 100 kHz to 100 mHz, frequency step 10 points per decade. All experiments were recorded in the dark and under visible-light illumination at 0.6 V vs an aqueous Ag/AgCl/3 M KCl reference electrode.

More details of the methods are given in the Supporting Information.

RESULTS AND DISCUSSION

In 2018, we demonstrated that the *in situ* self-assembly of tetrathiafulvalene (TTF), $TTF^{\bullet+}$, and BF_4^- or PF_6^- on the surface of Pt microparticles in wet acetonitrile is active for the WOR upon visible-light irradiation.[34] In short, we had demonstrated that $TTF^{\bullet+}$* is highly oxidizing and that the molecular assembly $TTF/TTF^{\bullet+}BF_4^-$, once photoexcited, can provide the four electrons required to oxidize water when it is dissolved in an organic solvent. However, this system is short-lived because it suffers from a gradual increase in the proton concentration in the wet organic phase and subsequent protonation of TTF in the molecular assemblies, triggering competing reactions such as proton and oxygen reduction[34] and preventing the electrochemical recycling of TTF back to $TTF^{\bullet+}$.

In this work, we eliminate the use of metallic catalysts for the WOR, replacing them with a low-cost, and highly stable, $TTF/TTF^{\bullet+}BF_4^-$@carbon junction, which works as an all-in-one redox-shuttle/photosensitizer/molecular-catalyst triad for the visible-light-driven WOR at neutral pH. Thus, we take advantage of the possibility of adjusting the Gibbs energy transfer across a polarized water|butyronitrile interface, to separate *in situ* and in a spontaneous manner the hydrophilic protons from the lipophilic TTF formed upon the visible-light-driven WOR by $TTF/TTF^{\bullet+}BF_4^-$ assemblies. The goal of such a separation is to prevent TTF from being protonated and therefore allow its electrochemical (*in situ*) reoxidation to perform continuous photosensitized WOR. Subsequently, the protons generated are chemically consumed in the cathodic compartment by redox electrocatalysis. Indeed, the standard redox potential of the V^{3+}/V^{2+} couple is −0.26 V and is therefore reducing enough to generate hydrogen on an electrocatalyst such as molybdenum carbide. Here, the strategy is to set up a "proton pump" to extract the photogenerated protons in the anodic compartment toward the cathodic compartment, where they are directly reduced to produce hydrogen. The reason to choose the V^{3+}/V^{2+} couple lies in the long experience that our group has in producing hydrogen on a very large scale using a vanadium redox flow battery (200 kW−400 kWh).[51−53] However, on consideration that our long-term objective is to develop a fully environmentally friendly WOR-HER system, the next step is to improve the HER part of the cell, replacing vanadium by a nonmetallic hydrogen evolution system, which is a work in progress in our laboratory.

Because the primary objective of this work is to demonstrate long-lived water photo-oxidation by $TTF/TTF^{\bullet+}BF_4^-$ assemblies on carbon electrodes without any metal catalyst, we chose to operate the electrochemical regeneration of $TTF^{\bullet+}$ from TTF at the carbon electrode by applying a constant anode potential using a potentiostat where the carbon electrode is the working electrode (see Scheme 2). The electrode in the aqueous compartment acts as a counter electrode, and its potential cannot be directly controlled. It is, of course, the locus of a reduction reaction such as the reduction of V^{3+} to V^{2+}.

Scheme 2 schematically shows the H-cell used to test the visible-light-driven WOR by $TTF/TTF^{\bullet+}$@RVC and $TTF/TTF^{\bullet+}$@GF junctions (anodes), coupled to the *in situ* electrochemical regeneration of $TTF^{\bullet+}$ in the anodic compartment, and the reduction of protons by V^{2+}/Mo_2C in the cathodic compartment, using Pt mesh as a cathode.

Once the visible-light-driven WOR is triggered by illumination of the anodic compartment, the protons that formed are transferred to the aqueous phase of the emulsion, while TTF is transferred to the organic phase, as it is poorly soluble in water, the salt $TTF^{\bullet+}BF_4^-$ being soluble in both phases. As the two septum-sealed compartments are physically connected by an aqueous glass wool plug, the protons are extracted to the

https://doi.org/10.1021/jacsau.1c00408
JACS Au 2021, 1, 2294−2302

cathodic compartment, where they are reduced by V^{2+}/Mo_2C to produce H_2. The glass wool plug avoids a convective mixture of $TTF^{\bullet+}$ and VCl_2. Indeed, the transfer of VCl_2 to the anodic compartment results in the quenching of the visible-light-driven WOR and, therefore, in the inhibition of oxygen evolution and proton production, as the oxidation of V^{2+} by $TTF^{\bullet+}$ is thermodynamically much more feasible than the oxidation of water.

In accordance with the CV recorded prior to the experiment (Figure 1), the onset current of the electrochemical WOR on the carbon electrode is observed beyond 1.15 V, and the electrochemical oxidation of TTF is observed above 0.4 V vs an Ag/AgCl/3 M KCl double-junction reference electrode. Therefore, we set the continuous recycling of $TTF^{\bullet+}$ at 0.6 V vs Ag/AgCl/3 M KCl, which is about 600 mV less positive than the potential required for the electrochemical WOR on the bare carbon electrode under the conditions of the experiment (Figure 1). It should also be noted that, in the absence of stirring, the two phases separate and the anode is then immersed only in the butyronitrile phase and that at this potential (0.6 V vs Ag/AgCl/3 M KCl) basically no aqueous species, including water, can be oxidized.

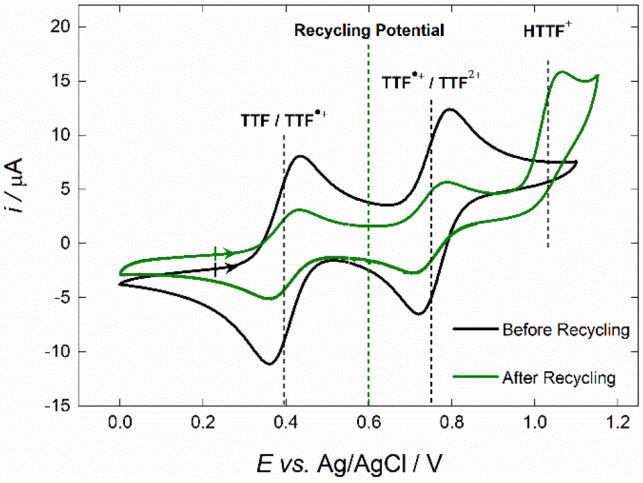

Figure 1. The black plot shows the cyclic voltammogram of the organic phase of the anodic compartment shown in Scheme 2 (1 mM $TTF^{\bullet+}$) prior to the experiment. The green plot corresponds to the CV obtained after 9 h of experiment for control 2: with $TTF^{\bullet+}$ in the anodic compartment but without V^{2+}/Mo_2C in the cathodic compartment and GF as the anode and Pt mesh as the cathode. The reference electrode and all the other conditions were the same as for the system in Scheme 2. A glassy-carbon electrode (D = 3 mm) was used as the WE, with 50 mM $TBABF_4$ as the supporting electrolyte. Scan rate: 25 mV s^{-1}.

As shown in Figure 2, the GC-MSD analyses of the gas accumulated in the headspace of the anodic compartment proved the continuous evolution of O_2 upon visible-light-driven WOR by the TTF/$TTF^{\bullet+}$@GF junction coupled to the electrochemical recycling of $TTF^{\bullet+}$. Similarly, the GC-TCD analyses of the headspace of the cathodic compartment showed the continuous evolution of H_2 upon reduction of the protons produced in the anodic compartment after they were transferred to the cathodic compartment. As expected for the stochiometric WOR, the experiment described in Scheme 2 produced on average 1 mol of O_2 per 2 mol of H_2. It is also important to note the high purity of the gases formed in both compartments. Indeed, the GC analyses showed that only O_2 was produced in the anodic compartment and only H_2 was produced in the cathodic compartment and they do not cross to the adjacent compartment during the experiment (Figure SI2).

Figure 3a shows the total number of H_2 moles produced and the yield of the WOR defined as $Y_{H2,WOR} = 2n_{150\ min}(H_2)/n_0(TTF^{\bullet+}) \times 100$, achieved after 150 min of visible-light driven WOR, constant anode potential electrolysis of TTF, and proton reduction (for more details on the calculation of the efficiencies see eqs SI3−SI6 in the Supporting Information). Figure 3a compares the activity of TTF/$TTF^{\bullet+}$@RVC and TTF/$TTF^{\bullet+}$@GF junctions. The TTF/$TTF^{\bullet+}$@RVC and the TTF/$TTF^{\bullet+}$@GF junctions achieved an impressive $Y_{H2,WOR} = 0.5 \times 10^5$% and 2.2×10^5% efficiencies, respectively, accounting for a recycling of $TTF^{\bullet+}$ of 530 and 2200 times, respectively. These results prove that the TTF/$TTF^{\bullet+}$@carbon systems alone act as a redox shuttle/photosensitizer/catalyst triad for the visible-light-driven WOR, without the need for any metallic catalyst.

As a control, a Pt mesh that yielded the same initial current as the GF electrode (Figure 3b) was also tested as an anode. This TTF/$TTF^{\bullet+}$@Pt junction reached half of the efficiency of the TTF/$TTF^{\bullet+}$@GF junction (Figure 3a). In addition, as shown in Figure 3b, the TTF/$TTF^{\bullet+}$@GF junction is electrochemically stable for as long as 5 h, while the stability of the TTF/$TTF^{\bullet+}$@Pt junction starts to decrease after 1 h of reaction.

The SEM-EDX analyses of the GF (Figure 4a−i) after constant visible-light-driven WOR and anode potential electrolysis of TTF show the self-assembly of micrometer-sized (0.3−2 μm) cauliflower-like arrays, composed by sulfur and fluorine (Figure 4b−i), indicating the self-assembly of TTF/$TTF^{\bullet+}BF_4^-$ on the surface of the GF. These arrays are likely to be the nuclei of the microtubes (0.1−0.5 μm) observed in Figure 4c−i, which are similar to the microtubes observed in our previous work on Pt microparticles in wet acetonitrile.[34] The size of the microtubes is consistent with the smaller diameter of the seminal graphite filaments (ca. 0.3 μm, Figure 4a). Indeed, Favier et al.[54] showed the slow electrocrystallization of $TTF(Br)_x$ conductive microtubes on Pt nanoparticles deposited on a GF electrode, whose diameters were directly proportional to the diameter of the Pt particles.

The growth of conductive TTF/$TTF^{\bullet+}$ microtubes on the surface of the GF observed by SEM explains the decrease in resistance of the electron transfer through the GF observed by EIS as the visible-light-driven WOR and electrochemical recycling of $TTF^{\bullet+}$ advanced (Figure 5).

In contrast, for the control where a Pt mesh was used as the anode instead of carbon, the SEM-EDX analyses showed the growth of a TTF-based film on the surface of Pt (Figure 4j,k), which correlates with the increase in capacitance of the TTF/$TTF^{\bullet+}$@Pt junction as the WOR advances (Figure 5). The EIS and SEM analyses show that the filamentary structure of the GF (electric conductivity 9.1×10^4 S m^{-1})[55] offers countless micrometer-sized seeds for the growth of TTF-based arrays, explaining the better performance of the TTF/$TTF^{\bullet+}$@GF junction in comparison with the flat Pt mesh that, although it exhibits a much higher conductivity (9×10^6 S m^{-1}), does not offer the micrometer-sized seeds required to grow the TTF-based conductive arrays.

After 5 h of reaction, both the current recorded during the electrochemical recycling of TTF to $TTF^{\bullet+}$ (Figure 3b) and the efficiency of the visible-light-driven WOR by the TTF/$TTF^{\bullet+}$@GF junction (Figure 3c) started to decrease due to passivation of the GF. At this point, we switched the light off and stopped the electrochemical process to replace the anode by a clean GF.

https://doi.org/10.1021/jacsau.1c00408
JACS Au 2021, 1, 2294−2302

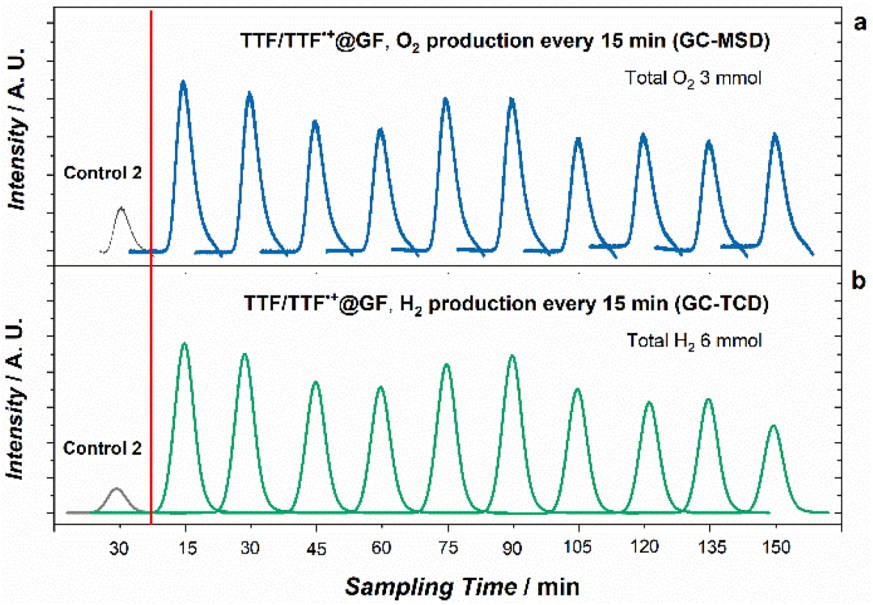

Figure 2. Analysis of the gas accumulated in the headspace of the two septum-sealed compartments of the H-cell depicted in Scheme 2 (anode, GF; cathode, Pt mesh; RE, Ag/AgCl/3 M KCl double junction). (a) Anodic compartment: production of O_2 upon visible-light-driven WOR by TTF/TTF$^{\bullet+}$@GF coupled to *in situ* constant anode potential electrolysis of TTF. (b) Cathodic compartment: production of H_2 upon continuous reduction of the protons produced in the anodic compartment. The left inset shows the gas measured during control 2. Each peak corresponds to the gas produced in each compartment every 15 min during a 150 min experiment (sampling time).

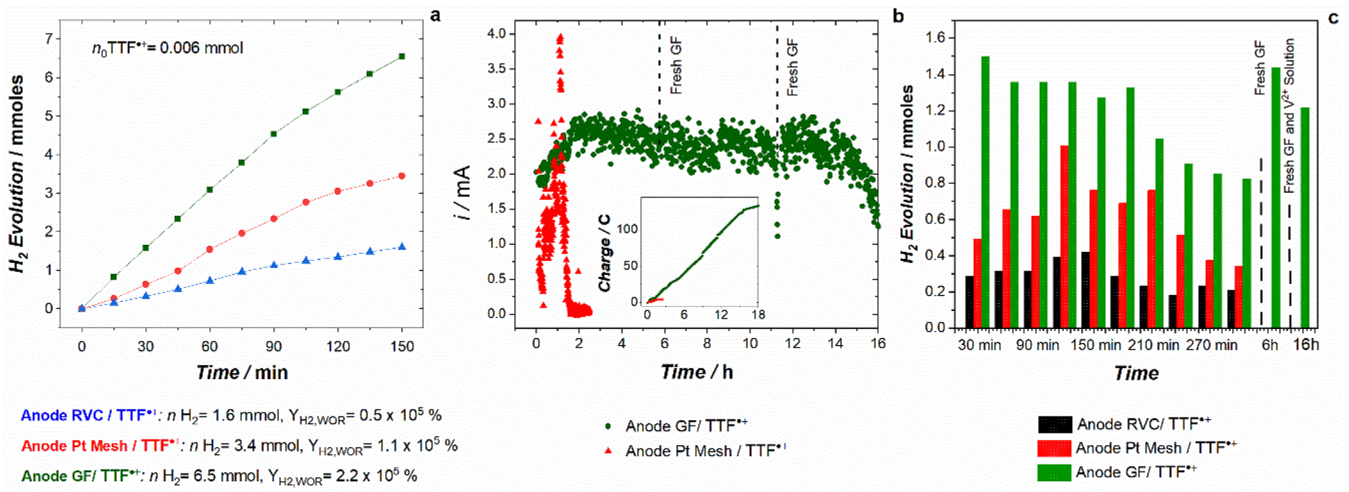

Figure 3. Analysis of the efficiency and stability of the TTF/TTF$^{\bullet+}$@RVC and TTF/TTF$^{\bullet+}$@GF (and TTF/TTF$^{\bullet+}$@Pt as control) junctions on the visible-light-driven WOR upon *in situ* constant anode potential electrolysis of TTF and continuous reduction of protons to H_2 (Scheme 2). (a) Overall H_2 production in the cathodic compartment. (b) Anode current vs time and charge vs time plots recorded during 16 h of the experiments performed with the TTF/TTF$^{\bullet+}$@Pt and TTF/TTF$^{\bullet+}$@GF junctions. When GF was used as the anode, the experiment was turned off every 5 h to change the anode for a new GF. Afterward, the experiment was turned back on. The time depicted in the plot corresponds only to the time during which the light and the recycling were on. (c) Production of H_2 quantified every 15 min during a 3 h long experiment for the three systems described in (a). The last column corresponds to an individual quantification after 16 h of recycling.

Once the light and the constant anode potential were turned back on, the current and efficiency recovered to their initial values (Figure 3b,c). The time depicted in Figures 3b,c corresponds to the time during which the light and the recycling were on. The used GF was then cleaned up with butyronitrile and used again, showing a total recovery of the activity.

This process was repeated three times up to 16 h (Figure 3b), exhibiting a stable current and a decrease of 15% in the efficiency of the WOR ($Y_{H2,WOR} = 1.1 \times 10^6$%), which is mainly due to the depletion of the V^{2+} solution, which was also replaced twice during the 16 h reaction. The fact that the whole system can be turned off and on without evident loss of efficiency and stability is a competitive advantage if the system is to be connected to an intermittent supply of energy. The stability of the TTF/TTF$^{\bullet+}$@GF junction upon continuous visible-light WOR and *in situ* constant anode potential electrolysis of TTF was further tested up to 100 h. The results of this experiment showed the constant production of gases, a constant current, and a constant charge increase (Figure SI3) proving the high stability of the photocatalytic system, which could indeed run further, as it did not show signs of decomposition.

https://doi.org/10.1021/jacsau.1c00408
JACS Au 2021, 1, 2294−2302

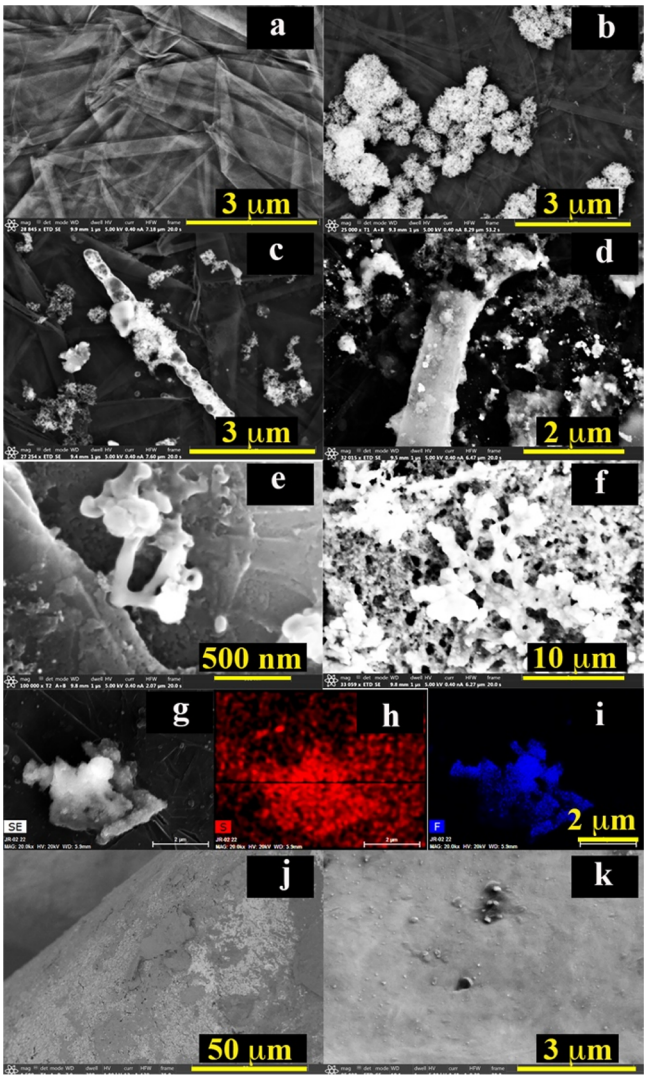

Figure 4. SEM analysis. (a) New GF cleaned with water and butyronitrile (ETD SE). (b–f) GF as the anode after 150 min of experiment (Scheme 2); T1D: bright area, higher atomic number (TTF); gray area, lower atomic number (carbon). (g) ETD SE: bright area, self-assembly; dark area, support (GF). (h) EDX composition: sulfur in red (TTF). (i). EDX: composition, fluorine in blue (BF_4). (j) Pt mesh as the anode after 150 min of constant anode potential electrolysis (Scheme 2). T1D: bright area, higher atomic number (Pt); gray area, lower atomic number (TTF-based film). (k) ETD SE: bright area, covering film; dark area, Pt mesh.

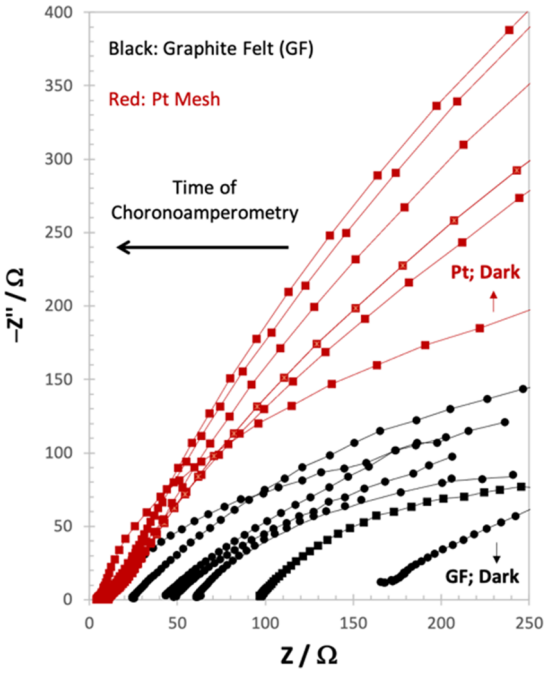

Figure 5. Electrochemical impedance spectra (EIS) recorded during the recycling of $TTF^{\bullet+}$ (constant anode potential electrolysis upon visible-light-driven WOR, Scheme 2). Each spectrum corresponds to 30 min of constant anode potential electrolysis starting from the experiment without light (dark). Prior to recording of the impedance spectra the stirring was turned off, and after the analysis the stirring was turned back on. Conditions: 10 mV amplitude perturbation, 100 kHz to 100 mHz, frequency step 10 points per decade. All experiments were recorded under visible-light illumination at 0.6 V vs an aqueous Ag/AgCl/3 M KCl reference electrode.

The main advantage of the electrochemical recycling of $TTF^{\bullet+}$ over the use of sacrificial electron acceptors is that no waste products which could decompose and eventually quench and slow down the WOR are produced.[37] Attempts of electrochemical recycling of other electron donors/acceptors have been unsuccessful due to their long-term instability.[16,56]

The UV absorption spectrum (Figure SI4) and MS (Figure SI5) show no evidence of decomposition of the TTF species, showing that the cell can operate on a long-term basis.

To prove that the visible-light-driven WOR is triggered by the $TTF/TTF^{\bullet+}$@GF junction alone and no other factor was taking place, two control experiments were performed.

Control 1 was made without $TTF^{\bullet+}$ in the anodic compartment, with V^{2+}/Mo_2C in the cathodic compartment, and using GF as the anode and Pt mesh as the cathode (all other conditions were the same as for Scheme 2). This experiment produced neither O_2 in the anodic compartment nor H_2 in the cathodic compartment, proving that, without the $TTF/TTF^{\bullet+}$ assemblies, the visible-light-driven WOR is not triggered in the system described in Scheme 2 and therefore no protons were produced to be reduced by V^{2+}/Mo_2C in the cathodic compartment, explaining the absence of H_2.

Control 2 was made with $TTF^{\bullet+}$ in the anodic compartment, without V^{2+}/Mo_2C in the cathodic compartment, and using GF as the anode and Pt mesh as the cathode (all the other conditions were the same as for Scheme 2). This blank produced a small amount of O_2 and H_2 in the anodic and cathodic compartments, respectively, accounting for a recycling of $TTF^{\bullet+}$ of only 35 times, which is far below the recycling achieved when V^{2+}/Mo_2C is used for the proton reduction (2200 times). In this blank, the protons obtained upon visible-light-driven WOR by the $TTF/TTF^{\bullet+}$@GF junction in the anodic compartment were reduced by the Pt mesh alone in the cathodic compartment; however, the pH was not sufficiently low to trigger efficient electrochemical reduction of protons on the Pt mesh at the potential applied during the recycling (0.6 V). The CV recorded after control 2 was performed (green plot in Figure 1) shows the total protonation of TTF upon accumulation of the protons formed during the visible-light-driven WOR by $TTF^{\bullet+}$ in the anodic compartment.

This explains why the recycling ceases. The oxidation potential of $HTTF^+$ is close to 1.05 V vs the Ag/AgCl/3 M KCl double-junction reference electrode, which is too high in comparison to the potential set for the oxidation of the

https://doi.org/10.1021/jacsau.1c00408
JACS Au 2021, 1, 2294–2302

photogenerated TTF to $TTF^{\bullet+}$ (0.6 V). Therefore, the protonation of TTF also stops the anode potential electrolysis, the current dropping to almost zero after only 30 min of the experiment. This control proves that, under the conditions of the experiment, the chemical reduction of protons by V^{2+}/Mo_2C is much more efficient than that of Pt alone.

The mechanism of the WOR by $TTF^{\bullet+}$ assemblies at neutral pH (eqs 1 and 2) is the reverse mechanism of that previously proposed for the slow four-electron reduction of oxygen to water by TTF assemblies in acidic pH (see ref 57). Indeed, in ref 57 it was computationally established that the self-assembly of TTF-$TTFH^+$ dimers could provide the four electrons required to reduce oxygen to water, which is in fact the opposite reaction to the four-electron oxidation of water to O_2 studied in this paper.[57] However, in ref 57 the self-assembly of TTF was not proved experimentally; therefore, this manuscript offers experimental proof of the computational mechanism proposed in 2011.[57] The mechanism proposed in ref 57 involves the helical tetramer $[TTF_4H_2]^{2+}$ formed by the interaction of two TTF-$TTFH^+$ dimers $[TTF_4H_2]^{2+}$ (eq 1), which delivers the four electrons needed for the reduction of oxygen to water.[57]

$$4TTF^{\bullet+*} + 2H_2O \rightleftharpoons [TTF_4H\cdots HO_2]^{2+} + 2H^+ \rightleftharpoons [TTF_4H_2\cdots O_2]^{2+} + 2H^+ \rightleftharpoons [TTF_4H_2]^{2+} + O_2 + 2H^+ \rightleftharpoons 4TTF + O_2 + 4H^+ \quad (1)$$

Electrochemical recycling of $TTF^{\bullet+}$ on GF:

$$4TTF \rightleftharpoons 4TTF^{\bullet+} + 4e^- \quad (2)$$

Indeed, $[TTF_4H_2]^{2+}$ binds O_2 to form a $[TTF_4H_2\cdots O_2]^{2+}$ intermediate that is converted into the more stable $[TTF_4H\cdots HO_2]^{2+}$ complex (eq 1).[57] The highly reactive $HO_2^{\bullet}$ and $TTF^{\bullet+}$ moieties of the $[TTF_4H\cdots HO_2]^{2+}$ complex combine and dissociate from the tetramer and get the needed protons from the solution to form two molecules of water.[57] Counteranion–cation complexes such as $(TTFH^+)_2(BF_4^-)_2$ exhibit cation–anion electrostatic interactions rather than direct interactions between the two $TTFH^+$ units.[57] This paper offers evidence of the formation of such a TTF-based assembly.

CONCLUSIONS

A water|butyronitrile emulsion was successfully used as a platform for the spontaneous separation of the products of the visible-light-driven WOR by self-assembled TTF/$TTF^{\bullet+}$@GF junctions at neutral pH. Such a separation allowed the successful and efficient electrochemical recycling of TTF back to $TTF^{\bullet+}$ at 0.6 V vs. Ag/AgCl/3 M KCl in the organic phase, while simultaneously performing the molecular photosensitized WOR. Moreover, the protons partitioned to the aqueous phase were reduced to H_2 by V^{2+} acting as electron donors on Mo_2C microparticles acting as redox electrocatalysts. This work shows that, as long as the $TTF^{\bullet+}$/TTF assemblies have an appropriate substrate with a small grain size to grow on, they do not need any metal or organometallic catalyst to perform the photosensitized WOR efficiently. In fact, the TTF/$TTF^{\bullet+}$@GF junction showed 2 times the efficiency and 5 times the stability of a TTF/$TTF^{\bullet+}$@Pt analogue. During 16 h of recycling, no decomposition of TTF was observed and H_2 was consistently produced, achieving a yield of H_2 production of 1.1×10^6% in relation to the initial concentration of $TTF^{\bullet+}$. Constant gas production, constant current, and constant increase of the charge were recorded during 100 h of visible-light-induced WOR and *in situ* constant anode potential electrolysis of TTF, and no signs of decomposition were observed, indicating that the recycling could be continued further. In conclusion, we have demonstrated a sustainable photosensitized WOR system operating in an emulsified system, where a TTF/$TTF^{\bullet+}$@GF junction performs as a photosensitizer/molecular-catalyst/redox-shuttle triad with the total absence of metallic or organometallic catalysts and sacrificial electron acceptors. This work opens new perspectives for sustainable metal-atom-free visible-light-driven water splitting in biphasic systems at neutral pH.

ASSOCIATED CONTENT

Supporting Information

The Supporting Information is available free of charge at https://pubs.acs.org/doi/10.1021/jacsau.1c00408.

Methods, mechanism of separation of the products of the visible-light-driven WOR by $TTF^{\bullet+}$, details on the role of vanadium in the proton reduction reaction, an analysis of the headspace of the two compartments of the H-cell depicted in Scheme 2 after 15 min of experiment, a 100 h study of the stability of the TTF/$TTF^{\bullet+}$@GF junction upon continuous visible-light WOR and *in situ* constant anode potential electrolysis of TTF, and the study of the stability of TTF by UV–vis absorption and mass spectrometry (PDF)

AUTHOR INFORMATION

Corresponding Authors

Astrid J. Olaya − *Laboratory of Physical and Analytical Electrochemistry, EPFL Valais Wallis, École Polytechnique Fédérale de Lausanne, CH-1951 Sion, Switzerland;* orcid.org/0000-0002-9770-130X; Email: astrid.olaya@epfl.ch

Hubert H. Girault − *Laboratory of Physical and Analytical Electrochemistry, EPFL Valais Wallis, École Polytechnique Fédérale de Lausanne, CH-1951 Sion, Switzerland;* orcid.org/0000-0001-5573-5774; Email: hubert.girault@epfl.ch

Authors

Julieta S. Riva − *Laboratory of Physical and Analytical Electrochemistry, EPFL Valais Wallis, École Polytechnique Fédérale de Lausanne, CH-1951 Sion, Switzerland; Consejo Nacional de Investigaciones Científicas y Técnicas, CONICET, Facultad de Matemática, Astronomía, Física y Computación, Universidad Nacional de Córdoba, Medina Allende s/n, Ciudad Universitaria, X5000HUA Córdoba, Argentina*

Dominika Baster − *Laboratory of Physical and Analytical Electrochemistry, EPFL Valais Wallis, École Polytechnique Fédérale de Lausanne, CH-1951 Sion, Switzerland*

Wanderson O. Silva − *Laboratory of Physical and Analytical Electrochemistry, EPFL Valais Wallis, École Polytechnique Fédérale de Lausanne, CH-1951 Sion, Switzerland;* orcid.org/0000-0003-0674-2366

François Pichard − *Laboratory of Physical and Analytical Electrochemistry, EPFL Valais Wallis, École Polytechnique Fédérale de Lausanne, CH-1951 Sion, Switzerland;* orcid.org/0000-0003-2877-3657

Complete contact information is available at: https://pubs.acs.org/10.1021/jacsau.1c00408

Notes

The authors declare no competing financial interest.

■ ACKNOWLEDGMENTS

The authors wish to acknowledge the Swiss Science Foundation SNSF grants 200021_175745, Photo Induced Charge Transfer Reaction at Molecular Interfaces, and 20SC-1_193608, Photoproduction of hydrogen in biphasic systems with electron donor recycling. We also thank Dr. Natalia Gasilova for her help with the MS analysis, and Danick Reynard for his help with the SEM analysis.

■ REFERENCES

(1) Moniz, S. J. A.; Shevlin, S. A.; Martin, D. J.; Guo, Z.-X.; Tang, J. Visible-Light Driven Heterojunction Photocatalysts for Water Splitting - a Critical Review. *Energy Environ. Sci.* **2015**, *8* (3), 731−759.

(2) Reece, S. Y.; Hamel, J. A.; Sung, K.; Jarvi, T. D.; Esswein, A. J.; Pijpers, J. J. H.; Nocera, D. G. Wireless Solar Water Splitting Using Silicon-Based Semiconductors and Earth-Abundant Catalysts. *Science* **2011**, *334* (6056), 645−648.

(3) Rausch, B.; Symes, M. D.; Chisholm, G.; Cronin, L. Decoupled Catalytic Hydrogen Evolution from a Molecular Metal Oxide Redox Mediator in Water Splitting. *Science* **2014**, *345* (6202), 1326−1330.

(4) Aratani, N.; Kim, D.; Osuka, A. Discrete Cyclic Porphyrin Arrays as Artificial Light-Harvesting Antenna. *Acc. Chem. Res.* **2009**, *42* (12), 1922−1934.

(5) Barber, J. Photosynthetic Energy Conversion: Natural and Artificial. *Chem. Soc. Rev.* **2009**, *38* (1), 185−196.

(6) Bard, A. J.; Fox, M. A. Artificial Photosynthesis: Solar Splitting of Water to Hydrogen and Oxygen. *Acc. Chem. Res.* **1995**, *28* (3), 141−145.

(7) Abe, R.; Sayama, K.; Arakawa, H. Significant Effect of Iodide Addition on Water Splitting into H_2 and O_2 over Pt-Loaded TiO_2 Photocatalyst: Suppression of Backward Reaction. *Chem. Phys. Lett.* **2003**, *371*, 360.

(8) Abe, R.; Sayama, K.; Domen, K.; Arakawa, H. A New Type of Water Splitting System Composed of Two Different TiO_2 Photocatalysts (Anatase, Rutile) and a IO_3-/I- Shuttle Redox Mediator. *Chem. Phys. Lett.* **2001**, *344* (3−4), 339−344.

(9) Abe, R.; Sayama, K.; Sugihara, H. Development of New Photocatalytic Water Splitting into H_2 and O_2 Using Two Different Semiconductor Photocatalysts and a Shuttle Redox Mediator IO_3-/I. *J. Phys. Chem. B* **2005**, *109* (33), 16052−16061.

(10) Sivula, K.; Formal, F. L.; Grätzel, M. WO_3-Fe_2O_3 Photoanodes for Water Splitting: A Host Scaffold, Guest Absorber Approach. *Chem. Mater.* **2009**, *21* (13), 2862−2867.

(11) Sivula, K.; Zboril, R.; Le Formal, F.; Robert, R.; Weidenkaff, A.; Tucek, J.; Frydrych, J.; Grätzel, M. Photoelectrochemical Water Splitting with Mesoporous Hematite Prepared by a Solution-Based Colloidal Approach. *J. Am. Chem. Soc.* **2010**, *132* (21), 7436−7444.

(12) Moon, S. J.; Baranoff, E.; Zakeeruddin, S. M.; Yeh, C. Y.; Diau, E. W. G.; Grätzel, M.; Sivula, K. Enhanced Light Harvesting in Mesoporous TiO_2/P_3HT Hybrid Solar Cells Using a Porphyrin Dye. *Chem. Commun.* **2012**, *47* (29), 8244−8246.

(13) Yu, Z.; Li, F.; Sun, L. Recent Advances in Dye-Sensitized Photoelectrochemical Cells for Solar Hydrogen Production Based on Molecular Components. *Energy Environ. Sci.* **2015**, *8* (3), 760−775.

(14) Yu, J.; Mathew, S.; Flavel, B. S.; Johnston, M. R.; Shapter, J. G. Ruthenium Porphyrin Functionalized Single-Walled Carbon Nanotube Arrays - A Step toward Light Harvesting Antenna and Multibit Information Storage. *J. Am. Chem. Soc.* **2008**, *130* (27), 8788−8796.

(15) Yu, Z.-Y.; Duan, Y.; Gao, M.-R.; Lang, C.-C.; Zheng, Y.-R.; Yu, S.-H. A One-Dimensional Porous Carbon-Supported Ni/Mo_2C Dual Catalyst for Efficient Water Splitting. *Chem. Sci.* **2017**, *8* (2), 968−973.

(16) Symes, M. D.; Cronin, L. Decoupling Hydrogen and Oxygen Evolution during Electrolytic Water Splitting Using an Electron-Coupled-Proton Buffer. *Nat. Chem.* **2013**, *5*, 403.

(17) Das, B.; Thapper, A.; Ott, S.; Colbran, S. B. Structural Features of Molecular Electrocatalysts in Multi-Electron Redox Processes for Renewable Energy - Recent Advances. *Sustain. Energy. Fuels* **2019**, *3* (9), 2159−2175.

(18) Chen, L.; Dong, X.; Wang, Y.; Xia, Y. Separating Hydrogen and Oxygen Evolution in Alkaline Water Electrolysis Using Nickel Hydroxide. *Nat. Commun.* **2016**, *7* (1), 11741.

(19) Adachi, M.; Okada, I.; Ngamsinlapasathian, S.; Murata, Y.; Yoshikawa, S. Dye-Sensitized Solar Cells Using Semiconductor Thin Film Composed of Titania Nanotubes. *Electrochemistry* **2002**, *70* (6), 449−452.

(20) Alivisatos, A. P. Semiconductor Clusters, Nanocrystals, and Quantm Dots. *Science* **1996**, *271*, 933.

(21) Chen, X. B.; Shen, S. H.; Guo, L. J.; Mao, S. S. Semiconductor-Based Photocatalytic Hydrogen Generation. *Chem. Rev.* **2010**, *110*, 6503.

(22) Hisatomi, T.; Kubota, J.; Domen, K. Recent Advances in Semiconductors for Photocatalytic and Photoelectrochemical Water Splitting. *Chem. Soc. Rev.* **2014**, *43* (22), 7520−7535.

(23) Kamat, P. V.; Tvrdy, K.; Baker, D. R.; Radich, J. G. Beyond Photovoltaics: Semiconductor Nanoarchitectures for Liquid-Junction Solar Cells. *Chem. Rev.* **2010**, *110* (11), 6664−6688.

(24) Campbell, W. M.; Jolley, K. W.; Wagner, P.; Wagner, K.; Walsh, P. J.; Gordon, K. C.; Schmidt-Mende, L.; Nazeeruddin, M. K.; Wang, Q.; Grätzel, M.; Officer, D. L. Highly Efficient Porphyrin Sensitizers for Dye-Sensitized Solar Cells. *J. Phys. Chem. C* **2007**, *111* (32), 11760−11762.

(25) Chen, K. S.; Liu, W. H.; Wang, Y. H.; Lai, C. H.; Chou, P. T.; Lee, G. H.; Chen, K.; Chen, H. Y.; Chi, Y.; Tung, F. C. New Family of Ruthenium-Dye-Sensitized Nanocrystalline TiO_2 Solar Cells with a High Solar-Energy-Conversion Efficiency. *Adv. Funct. Mater.* **2007**, *17* (15), 2964−2974.

(26) Feldt, S. M.; Gibson, E. A.; Gabrielsson, E.; Sun, L.; Boschloo, G.; Hagfeldt, A. Design of Organic Dyes and Cobalt Polypyridine Redox Mediators for High-Efficiency Dye-Sensitized Solar Cells. *J. Am. Chem. Soc.* **2010**, *132* (46), 16714−16724.

(27) Fu, X.; Xie, M.; Luan, P.; Jing, L. Effective Visible-Excited Charge Separation in Silicate-Bridged ZnO/$BiVO_4$ Nanocomposite and Its Contribution to Enhanced Photocatalytic Activity. *ACS Appl. Mater. Interfaces* **2014**, *6* (21), 18550−18557.

(28) Ho-Kimura, S.; Moniz, S. J. A.; Handoko, A. D.; Tang, J. Enhanced Photoelectrochemical Water Splitting by Nanostructured $BiVO_4$-TiO_2 Composite Electrodes. *J. Mater. Chem. A* **2014**, *2* (11), 3948−3953.

(29) Hong, S. J.; Lee, S.; Jang, J. S.; Lee, J. S. Heterojunction $BiVO_4$/WO_3 Electrodes for Enhanced Photoactivity of Water Oxidation. *Energy Environ. Sci.* **2011**, *4* (5), 1781−1787.

(30) Kudo, A.; Ueda, K.; Kato, H.; Mikami, I. Photocatalytic O_2 Evolution under Visible Light Irradiation on $BiVO_4$ in Aqueous $AgNO_3$ Solution. *Catal. Lett.* **1998**, *53* (3), 229−230.

(31) Pihosh, Y.; Turkevych, I.; Mawatari, K.; Asai, T.; Hisatomi, T.; Uemura, J.; Tosa, M.; Shimamura, K.; Kubota, J.; Domen, K.; Kitamori, T. Nanostructured WO_3/$BiVO_4$ Photoanodes for Efficient Photoelectrochemical Water Splitting. *Small* **2014**, *10* (18), 3692−3699.

(32) Bignozzi, C. A.; Caramori, S.; Cristino, V.; Argazzi, R.; Meda, L.; Tacca, A. Nanostructured Photoelectrodes Based on WO_3: Applications to Photooxidation of Aqueous Electrolytes. *Chem. Soc. Rev.* **2013**, *42* (6), 2228−2246.

(33) Bi, Y.; Ouyang, S.; Cao, J.; Ye, J. Facile Synthesis of Rhombic Dodecahedral AgX/Ag_3PO_4 (X = Cl, Br, I) Heterocrystals with Enhanced Photocatalytic Properties and Stabilities. *Phys. Chem. Chem. Phys.* **2011**, *13* (21), 10071−10075.

(34) Olaya, A. J.; Omatsu, T.; Hidalgo-Acosta, J. C.; Riva, J. S.; Bassetto, V. C.; Gasilova, N.; Girault, H. H. A Self-Assembled Organic/Metal Junction for Water Photo-Oxidation. *J. Am. Chem. Soc.* **2019**, *141* (16), 6765−6774.

(35) Olaya, A. J.; Hidalgo-Acosta, J. C.; Omatsu, T.; Girault, H. H. Photosensitized Hydrogen Evolution on a Floating Electrocatalyst

https://doi.org/10.1021/jacsau.1c00408
JACS Au 2021, 1, 2294−2302

Coupled to Electrochemical Recycling. *J. Am. Chem. Soc.* **2018**, *140* (32), 10149−10152.
(36) Peljo, P.; Scanlon, M. D.; Olaya, A. J.; Rivier, L.; Smirnov, E.; Girault, H. H. Redox Electrocatalysis of Floating Nanoparticles: Determining Electrocatalytic Properties without the Influence of Solid Supports. *J. Phys. Chem. Lett.* **2017**, *8* (15), 3564−3575.
(37) Schneider, J.; Bahnemann, D. W. Undesired Role of Sacrificial Reagents in Photocatalysis. *J. Phys. Chem. Lett.* **2013**, *4* (20), 3479−3483.
(38) Mirzakulova, E.; Khatmullin, R.; Walpita, J.; Corrigan, T.; Vargas-Barbosa, N. M.; Vyas, S.; Oottikkal, S.; Manzer, S. F.; Hadad, C. M.; Glusac, K. D. Electrode-Assisted Catalytic Water Oxidation by a Flavin Derivative. *Nat. Chem.* **2012**, *4* (10), 794−801.
(39) Li, H.; Xie, F.; Zhang, M.-T. Metal-Free Electrocatalyst for Water Oxidation Initiated by Hydrogen Atom Transfer. *ACS Catal.* **2021**, *11* (1), 68−73.
(40) Datta, A.; Kapri, S.; Bhattacharyya, S. Carbon Dots with Tunable Concentrations of Trapped Anti-Oxidant as an Efficient Metal-Free Catalyst for Electrochemical Water Oxidation. *J. Mater. Chem. A* **2016**, *4* (38), 14614−14624.
(41) Bigot, J.; Charleux, B.; Cooke, G.; Delattre, F.; Fournier, D.; Lyskawa, J.; Sambe, L.; Stoffelbach, F.; Woisel, P. Tetrathiafulvalene End-Functionalized Poly(N-Isopropylacrylamide): A New Class of Amphiphilic Polymer for the Creation of Multistimuli Responsive Micelles. *J. Am. Chem. Soc.* **2010**, *132* (31), 10796−10801.
(42) Giffard, M.; Gorgues, A.; Riou, A.; Roncali, J.; Alonso, P.; Uriel, S.; GarÌn, J.; Nguyen, T. P. Generation of Radicals and Formation of Conducting Materials by Protic Doping of Tetrahiafulvalenes. *Synth. Met.* **1995**, *70*, 1133−1134.
(43) Akutagawa, T.; Kakiuchi, K.; Hasegawa, T.; Noro, S.-I.; Nakamura, T.; Hasegawa, H.; Mashiko, S.; Becher, J. Molecularly Assembled Nanostructures of a Redox-Active Organogelator. *Angew. Chem., Int. Ed.* **2005**, *44* (44), 7283−7287.
(44) Halling, M. D.; Bell, J. D.; Pugmire, R. J.; Grant, D. M.; Miller, J. S. Solid-State NMR Spectra and Long, Intra-Dimer Bonding in the $(\text{-}[\text{TTF}]_2^{2+}$ (TTF = Tetrathiafulvalene) Dication. *J. Phys. Chem. A* **2010**, *114* (24), 6622−6629.
(45) Sun, W.; Xu, C.-H.; Zhu, Z.; Fang, C.-J.; Yan, C.-H. Chemical-Driven Reconfigurable Arithmetic Functionalities within a Fluorescent Tetrathiafulvalene Derivative. *J. Phys. Chem. C* **2008**, *112* (43), 16973−16983.
(46) Kobayashi, Y.; Yoshioka, M.; Saigo, K.; Hashizume, D.; Ogura, T. Hydrogen-Bonding-Assisted Self-Doping in Tetrathiafulvalene (TTF) Conductor. *J. Am. Chem. Soc.* **2009**, *131* (29), 9995−10002.
(47) Wenger, S.; Bouit, P.-A.; Chen, Q.; Teuscher, J.; Censo, D. D.; Humphry-Baker, R.; Moser, J.-E.; Delgado, J. L.; Martin, N.; Zakeeruddin, S. M.; Grätzel, M. Efficient Electron Transfer and Sensitizer Regeneration in Stable t-Extended Tetrathiafulvalene-Sensitized Solar Cells. *J. Am. Chem. Soc.* **2010**, *132* (14), 5164−5169.
(48) Sun, L.; Campbell, M. G.; Dincă, M. Electrically Conductive Porous Metal-Organic Frameworks. *Angew. Chem., Int. Ed.* **2016**, *55* (11), 3566−3579.
(49) Jana, A.; Bähring, S.; Ishida, M.; Goeb, S.; Canevet, D.; Sallé, M.; Jeppesen, J. O.; Sessler, J. L. Functionalised Tetrathiafulvalene- (TTF-) Macrocycles: Recent Trends in Applied Supramolecular Chemistry. *Chem. Soc. Rev.* **2018**, *47* (15), 5614−5645.
(50) Legros, J.-P.; Bousseau, M.; Valade, L.; Cassoux, P. Crystal Structure of a Non-Conductive Non-Stoichiometric Tetrathiafulvalenium Salt: $(TTF)_3(BF4)_2$. *Mol. Cryst. Liq. Cryst.* **1983**, *100* (1−2), 181−192.
(51) Peljo, P.; Vrubel, H.; Amstutz, V.; Pandard, J.; Morgado, J.; Santasalo-Aarnio, A.; Lloyd, D.; Gumy, F.; Dennison, C. R.; Toghill, K. E.; Girault, H. H. All-Vanadium Dual Circuit Redox Flow Battery for Renewable Hydrogen Generation and Desulfurisation. *Green Chem.* **2016**, *18* (6), 1785.
(52) Amstutz, V.; Toghill, K. E.; Powlesland, F.; Vrubel, H.; Comninellis, C.; Hu, X.; Girault, H. H. Renewable Hydrogen Generation from a Dual-Circuit Redox Flow Battery. *Energy Environ. Sci.* **2014**, *7* (7), 2350−2358.
(53) Reynard, D.; Girault, H. Combined Hydrogen Production and Electricity Storage Using a Vanadium-Manganese Redox Dual-Flow Battery. *Cell Reports Physical Science* **2021**, *2*, 100556.
(54) Favier, F.; Liu, H.; Penner, R. M. Size-Selective Growth of Nanoscale Tetrathiafulvalene Bromide Crystallites on Platinum Particles. *Adv. Mater.* **2001**, *13*, 1567−1570.
(55) Castañeda, L. F.; Walsh, F. C.; Nava, J. L.; Ponce de León, C. Graphite Felt as a Versatile Electrode Material: Properties, Reaction Environment, Performance and Applications. *Electrochim. Acta* **2017**, *258*, 1115−1139.
(56) Norris, M. R.; Cossairt, B. M. CdSe on a Mesoporous Transparent Conducting Oxide Scaffold as a Photocathode. *J. Mater. Chem. A* **2015**, *3* (28), 14585−14591.
(57) Olaya, A. J.; Ge, P.; Gonthier, J. F.; Pechy, P.; Corminboeuf, C.; Girault, H. H. Four-Electron Oxygen Reduction by Tetrathiafulvalene. *J. Am. Chem. Soc.* **2011**, *133* (31), 12115−12123.

https://doi.org/10.1021/jacsau.1c00408
JACS Au 2021, 1, 2294−2302